Materials Science in Semiconductor Processing 107 (2020) 104806

Contents lists available at ScienceDirect

Materials Science in Semiconductor Processing

journal homepage: http://www.elsevier.com/locate/mssp

Characterization of RuO_2–Rh_2O_3 supported on $Ag_{1-x}NbO_3$; at x=0, 0.1 and 0.5 for the H_2 production

Arquímedes Cruz-López [a,*], Santiago Iván Suárez-Vázquez [a], Dora Alicia Solís-Casados [b], Carlos Alberto Ramos-Rivera [a], Rodolfo Zanella [c]

[a] Universidad Autónoma de Nuevo León, Facultad de Ingeniería Civil, Av. Universidad S/N, San Nicolás de los Garza Nuevo León, 66455, Mexico
[b] Universidad Autónoma del Estado de México, Facultad de Química, Centro Conjunto de Investigación en Química Sustentable UAEM-UNAM, Carretera Toluca-Atlacomulco km 14.5, San Cayetano, 50120, Toluca, Mexico
[c] Instituto de Ciencias Aplicadas y Tecnología, Universidad Nacional Autónoma de México, Circuito Exterior S/N, C.U., Ciudad de México, 04510, Mexico

ARTICLE INFO

Keywords:
Niobates
Semiconductor
Catalyst Ru–Rh
Electrocatalysis

ABSTRACT

In this work, the characterization of the RuO_2–Rh_2O_3 system supported on $Ag_{1-x}NbO_3$ (where x = 0, 0.1, and 0.5) prepared by the solid-state route at 900 °C for its employment as semiconductor in the production of hydrogen is presented. The physicochemical characterization evidences that the structural and electronic differences in the support were observed when the content of silver diminished by 50%. By X-ray diffraction of $AgNbO_3$ stoichiometric ratio is confirmed, while the support, where there is a diminution of the silver content, evolved toward $Ag_2Nb_2O_{11}$ mixed with the $AgNbO_3$ with a band gap toward the visible region (2.5 eV). The results of scanning electron microscopy confirmed the presence of particles with sizes lower than 10 nm in both cases. Impregnation of the Ru–Rh bimetallic phase indicates that the amount of dispersed ruthenium compounds (RuO_2, $RuRh_2O_4$ and $RuNbO_4$) were greater than the nominal charge ($1.40 > RuO_2/Rh_2O_3 < 2.83$). The electrochemical evaluation revealed a performance of 2.5-times greater for the 5%RuO_2-3% $Rh_2O_3/Ag_{0.5}NbO_3$ with respect to its homologue: 5%RuO_2-3% $Rh_2O_3/AgNbO_3$.

1. Introduction

Due to the diminution of the oil reserves in Mexico, the government has modified the energy policies to increase the exploitation of crude oil in deep waters, in addition to diversify the basic study and the exploitation of renewable energy [1]. Solar energy comprises a convincing alternative in terms of the needs of the planet, because it is a source of clean, inexhaustible energy, which is easily available in the majority of countries, which distances it from geopolitical tension. Additionally, it does not pose any environmental threat due to contamination or the emission of gases involved in the greenhouse effect [2].

The production of hydrogen by means of the reaction of water splitting promises to be a way to take advantage of the greatest energy source available on planet earth because, if the amount of energy radiated by the sun on the earth in 1 h (4.3E2 J) with respect to the total energy consumed on the planet in 1 year (4.1E20 J), it is very clear that this route can be taken advantage of as a finite source [3]. Unfortunately, present technological developments can capture less than 2% of these resources [3,4]; thus, it is necessary to advance in the design and manipulations of materials at the nanometric level in order to increase their efficiency and to take advantage more effectively of the greatest amount of solar energy. The latter justifies the importance of their study of semiconductors as a means to transform solar energy into chemical energy [5], in this manner reducing the growing demand for innocuous fuels and to diminish the effects of global warming, which are increasingly perceptible by our senses [1,2].

Since Fijushima and Honda reported the use of titanium dioxide (TiO_2) as a semiconductor material, with the capacity to dissociate the water molecule into atomic hydrogen and oxygen, through the action of UltraViolet (UV) light, an important number of reviews and articles have been published that associate progress in the optical properties of the different families of materials, such as oxides [6,7], nitrides [8–10], sulfides [11], and chalcogenides [12], in the water splitting reaction. However, each of these families has its own limitations; for example, the metallic oxides have preserved their use in the UV region, the chalcogenides are materials with a propensity toward photocorrosion and in turn the release of toxic metals or, in the case of mixed oxides, the combination of sensitivity to visible light, with a low potential of the

* Corresponding author.
E-mail address: cruzlopeza2015@gmail.com (A. Cruz-López).

https://doi.org/10.1016/j.mssp.2019.104806
Received 2 September 2019; Received in revised form 21 October 2019; Accepted 26 October 2019
Available online 16 November 2019

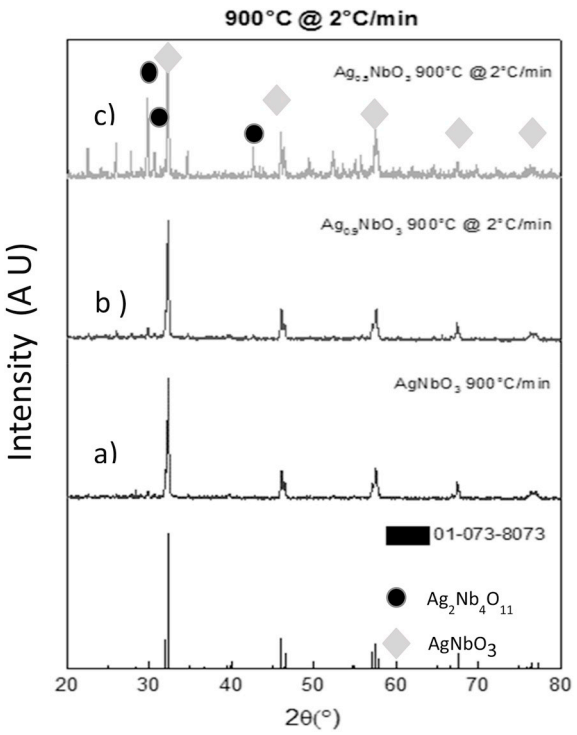

Fig. 1. X-ray diffraction of the samples of $AgNbO_3$ prepared by the solid-state route at 900 °C for 12 h. (a) $AgNbO_3$, (b) $Ag_{0.9}NbO_3$, and (c) $Ag_{0.5}NbO_3$ and JCPD 01–073–8073 card.

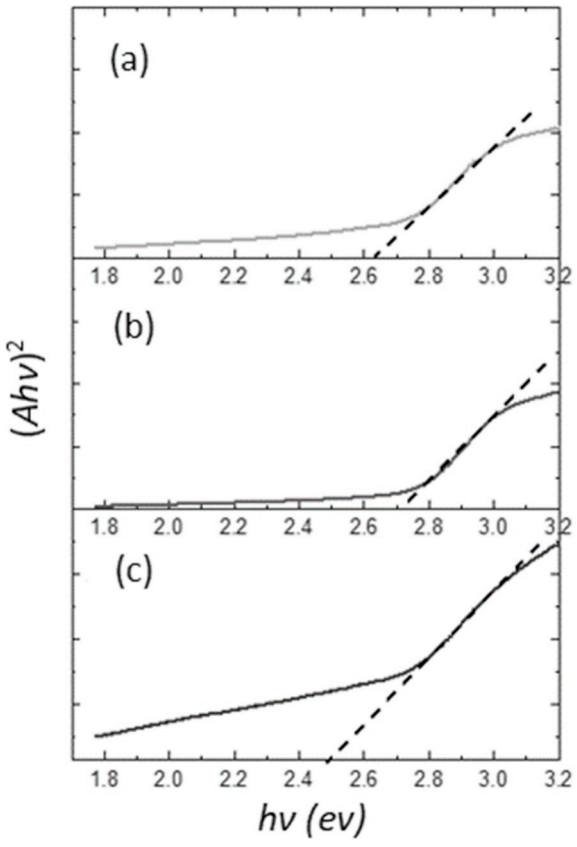

Fig. 2. Band gap energy of the samples $Ag_{1-x}NbO_3$; x = 0, 0.1, and 0.5 synthesized by the solid-state reaction at 900 °C/12 h. (a) $AgNbO_3$, (b) $Ag_{0.9}NbO_3$, and (c) $Ag_{0.5}NbO_3$.

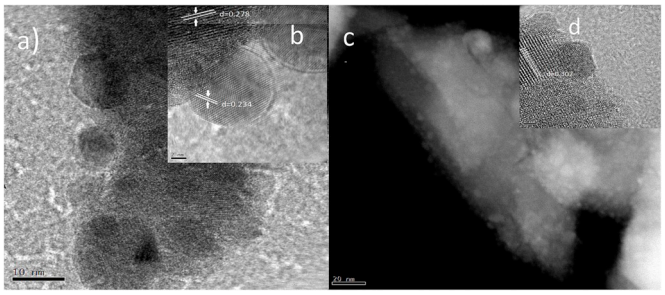

Fig. 3. Images of the Transmission Electronic Microscopy (TEM) of $Ag_{1-x}NbO_3$ supports x = 0, 0.1 and 0.5 synthesized at 900 °C by the solid-state reaction. (a-b) $AgNbO_3$ and (c-d) $Ag_{0.5}NbO_3$.

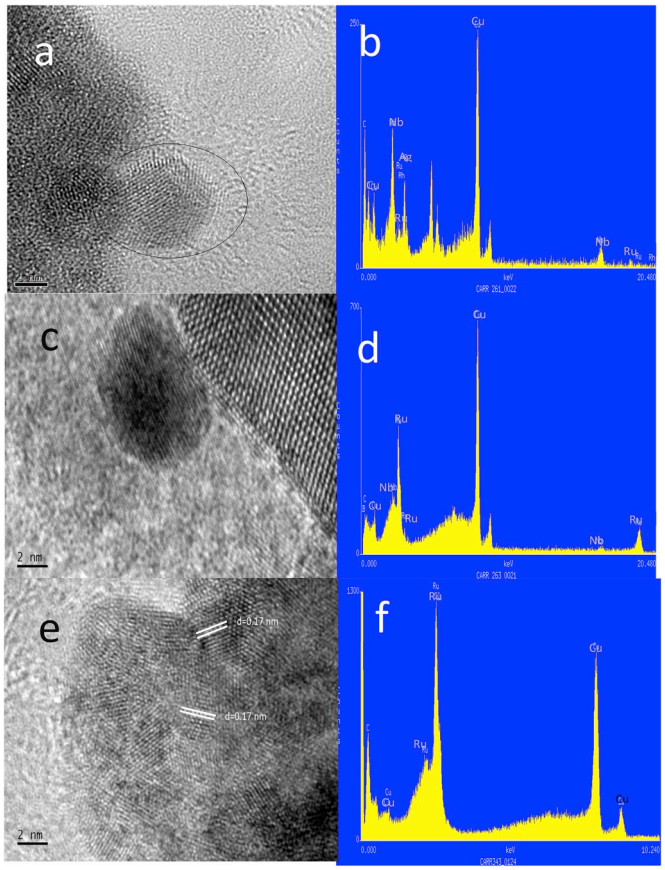

Fig. 4. Transmission Electronic Microscopy with EDS analysis of the systems of the bimetallic catalysts calcined at 400 °C/1 h. (a-b) 1%RuO_2–3%Rh_2O_3/$AgNbO_3$, (c-d) 3%RuO_2-3% Rh_2O_3/$Ag_{0.5}NbO_3$, and (e-f) 3%RuO_2-3% Rh_2O_3/$Ag_{0.5}NbO_3$.

conduction band that is insufficient for reducing the water into H_2 [13]. However, the alkaline niobates with an $AB_2Nb_3O_{10}$, laminar structure where A = K, Rb, Na, and Cs; B=Ca, Sr are considered promising materials for the photocatalytic generation of hydrogen; nonetheless, their low photocatalytic efficiency is associated with rapid recombination and the band gap limits their use on the visible region [14]. In contrast, niobates with a perovskite-type structure ($ANbO_3$, where A = Cu, Ag, and Au) present band gap of 2.7 eV and they are more promising [8].

The major challenges so far in the technology of artificial photosynthesis reactions are serious electron-hole recombination in bulk semiconductors photocatalysts and low adsorption on semiconductor surfaces [15,16]. In view of this restriction, the most frequent alternative is the decoration with metallic nanoparticles, such as Pt [15], Ag

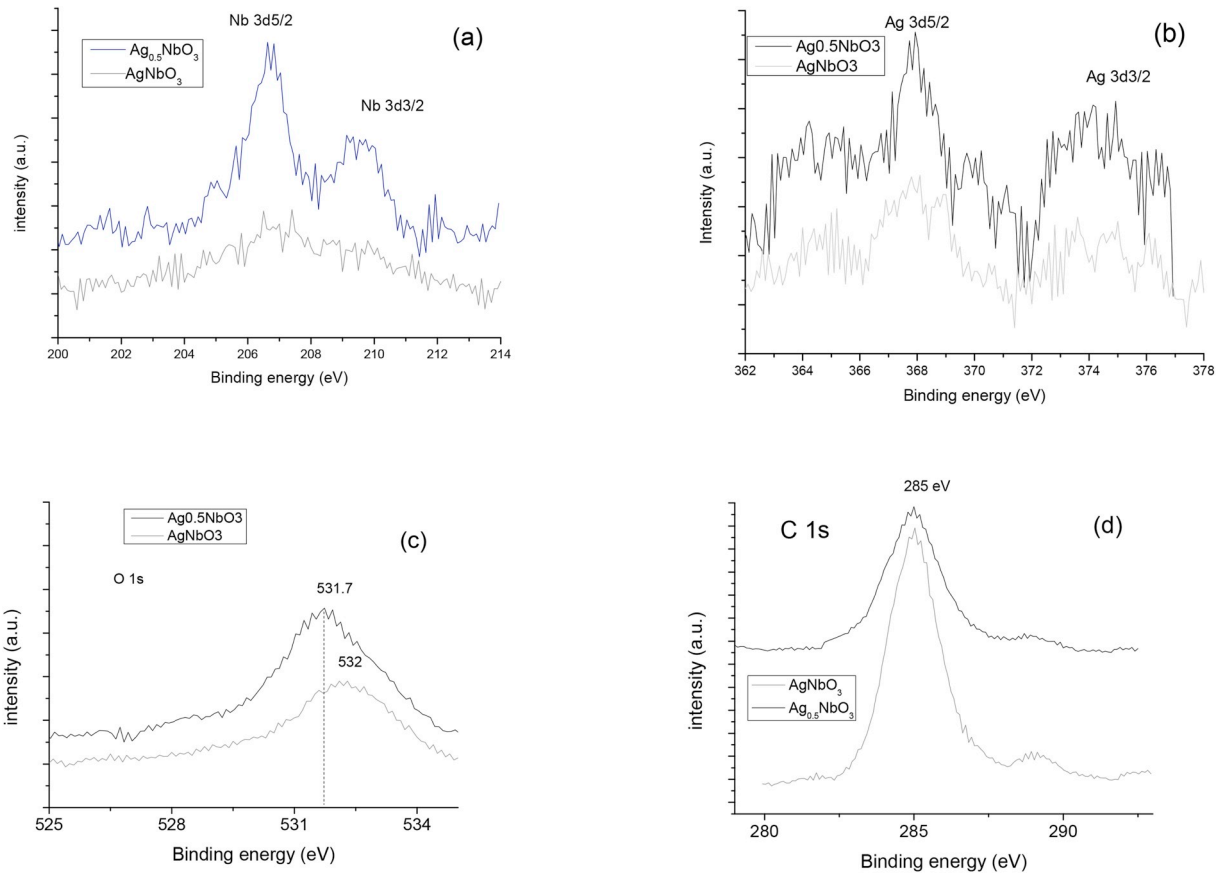

Fig. 5. XPS narrow spectra of silver niobates ($AgNbO_3$ and $Ag_{0.5}NbO_3$) prepared by the solid-state route and calcined at 900 °C/8 h. (a) Nb 3d5/2, (b) Ag 3d5/2, (c) O 1s and (d) C1s regions.

[17], Ru [18] and Rh [16,19] on the semiconductor surface for improve photocatalytic water splitting efficiency. The goals are i) metal co-catalyst trap the photogenerated electrons from semiconductor in promoting the electron hole separation and ii) the surface of cocatalysts offers highly reactive sites in promoting the adsorption and the photogenerated electrons reduce water to form H_2 while holes oxidize water to form O_2 on the oxide support. Nowadays, the most frequent case is decoration with metallic nanoparticles, which leads to an important increase of photocatalytic efficiency in the production of hydrogen [17, 20] or the degradation of methyl blue employing NiO/$AgNbO_3$ [21]. On the other hand, Yang Lu reported *in-situ* growth of Ag nanoparticles on $AgNbO_3$ by the action of light, with the purpose of improving the interaction of the Ag–$AgNbO_3$ interface, achieving interesting results for future applications in the treatment of residual waters [17].

In this work, an exploratory study is proposed on the effect of the RuO_2–Rh_2O_3 active phase distributed on the surface of the $Ag_{1-x}NbO_3$ system with X = 0, 1, and 0.5, with the purpose of understanding better the interaction of the metallic oxides during the electrochemical reaction for the production of hydrogen.

2. Experimental proccedure

2.1. Synthesis of niobates

Preparation of the $AgNbO_3$ was carried out from niobium oxide (Nb_2O_3, Sigma-Aldrich 99.99%) and silver obtained by electrolytical process (Ag^{1+}) as precursors. The electrolytic silver was pulverized into a ball-mill in order to obtain a desirable powder, and later, mixed in stoichiometric amount with respect to the mass of niobium oxide. Then, two mL was immediately added of acetone/methyl alcohol solution, at a 1:0.5 ratio to the powders, to render the paste more workable, the latter was triturated during 1 h to ensure homogeneity. Once the time had passed, the paste was left to dry at room temperature and a thermal treatment was carried out at 900 °C in a Thermo Scientific Thermolyne 200 muffler, with a heating ramp of 2 °C.min^{-1} in an air atmosphere.

For the case of synthesis with a non-stoichiometric ratios at 900 °C ($Ag_{1-x}NbO_3$ where X = 0.1, and 0.5), the experimental procedure is the same, except that the ratio of the silver mass varied with respect to the metallic oxide.

2.2. Impregnation of the Ru and Rh

The supports of silver niobates $Ag_{1-x}NbO_3$ where x = 0, 0.1 and 0.5 were impregnated with a triruthenium dodecacarbonyl precursor [$Ru_3(CO_{12})$, Sigma-Aldrich]. Each of the supports was decorated with theoretical metallic supports of RuO_2 = 1, 3, and 5%wt according to the following procedure: 0.5 g of silver niobate was weighed and, based on this amount, the weighed proportion was calculated of the [$Ru_3(CO_{12})$] necessary for each impregnation. The two solids were mixed in a glass containing 50 mL of TetraHydroFuran (THF; Sigma-Aldrich). The solution was maintained under mechanical agitation 0.5 h, and later, we proceeded to eliminate the THF, heating the solution to 60 °C. The recovered solids were dried in a furnace at 400 °C during 1 h to ensure the formation of the monometallic photocatalyst.

To obtain the Ru–Rh catalysts, all of the niobates were co-impregnated with metallic charges of 1, 3, and 5% of theoretical RuO_2 were co-impregnated with a metallic charge of rhodium (3%wt). For this case, we utilized Rh ([acac]$_3$), that is, rhodium acetylacetonate, and methyl alcohol (CH_3OH) as solvent. The same incipient wetness procedure was employed to obtain the bimetallic catalysts.

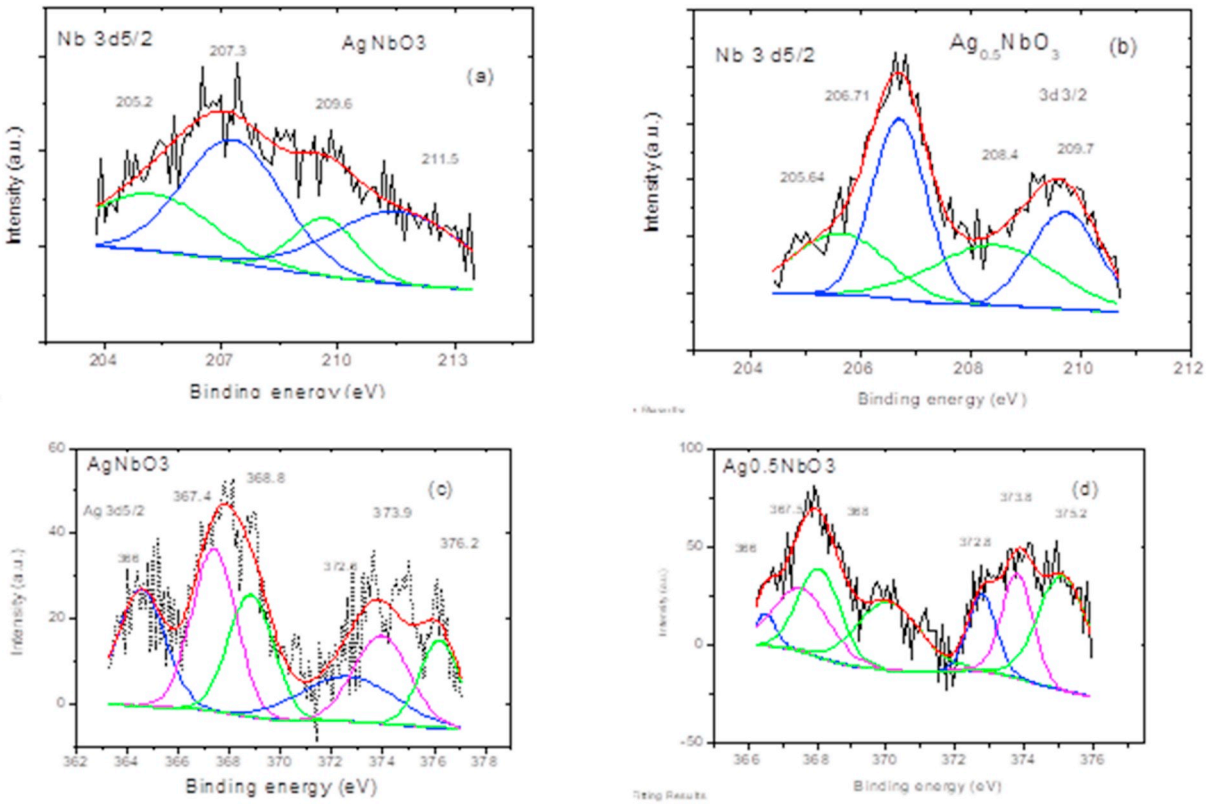

Fig. 6. XPS deconvoluted narrow spectra of silver niobates (a) Nb 3d5/2, in $AgNbO_3$ (b) Nb 3d5/2 in $Ag_{0.5}NbO_3$ (c) Ag 3d5/2 in $AgNbO_3$ (d) Ag 3d5/2 in $Ag_{0.5}NbO_3$.

Table 1
Elemental chemical composition of the bimetallic catalyst designed in this work.

Catalyst	Theoretical RuO_2/Rh_2O_3	XPS RuO_2/Rh_2O_3
1%RuO_2–3Rh_2O_3/$AgNbO_3$	0.17	1.42
3%RuO_2–3 Rh_2O_3/$AgNbO_3$	0.52	1.40
5%RuO_2–3 Rh_2O_3/$AgNbO_3$	0.87	2.83
1%RuO_2–3 Rh_2O_3/$Ag_{0.5}NbO_3$	0.17	1.32
3%RuO_2–3 Rh_2O_3/$Ag_{0.5}NbO_3$	0.52	1.17
5%RuO_2–3 Rh_2O_3/$Ag_{0.5}NbO_3$	0.87	0.95

2.3. Physicochemical characterization of supports and catalysts

Characterization of the silver niobates prepared by solid state at 900 °C was performed utilizing the x-ray diffraction technique (XRD), using PANalytical X'pert pro equipment, with Cu Kα radiation. Afterward, supports were characterized by 380 UV–vis Nicolet spectrophotometer, equipped with a diffuse reflectance accessory, with an integration sphere (Spectralon model) and transformed utilizing the following equation: $(F(R).hv)^2$, to know the band gap. Morphological characterization of the prepared catalyst, as well as chemical composition were determined by Transmission Electronic Microscopy (TEM) with Energy Dispersion Spectroscopy (EDS), employing a JEM model 2010 microscope. Additionally, the presence of the bimetallic phase (Ru–Rh) was confirmed by high resolution spectra obtained by X-ray photoelectron spectroscopy, utilizing JEOL 9200 equipment; with a source of Mg Kα. Correction of the charge displacement was conducted using the carbon peak localized at 285 eV (1s) as standard. The spectra were deconvoluted employing Origin version 8.2 software and using a Shirley-type baseline subtraction.

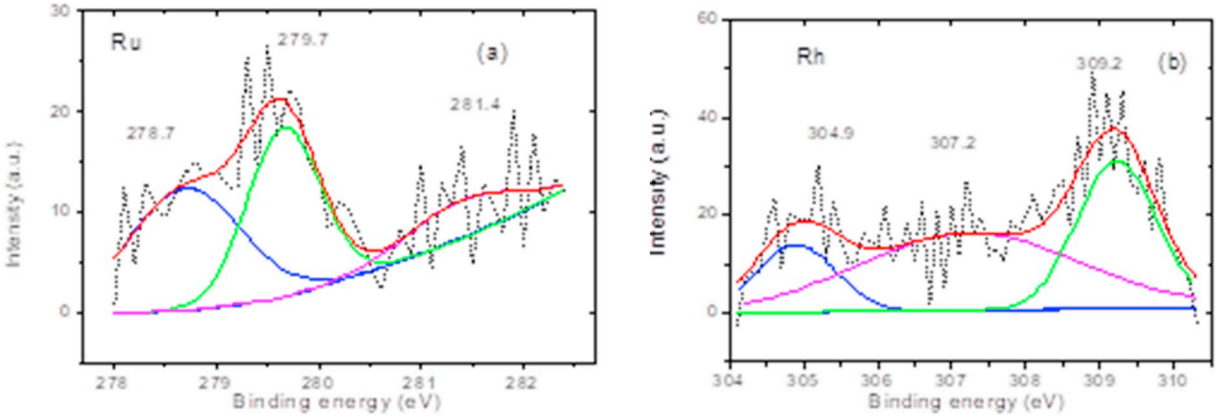

Fig. 7. XPS analysis of the 1%RuO_2–3Rh_2O_3/$AgNbO_3$ catalysts prepared by incipient wetness impregnation and calcined at 450 °C/8 h. (a) Ru and (b) Rh.

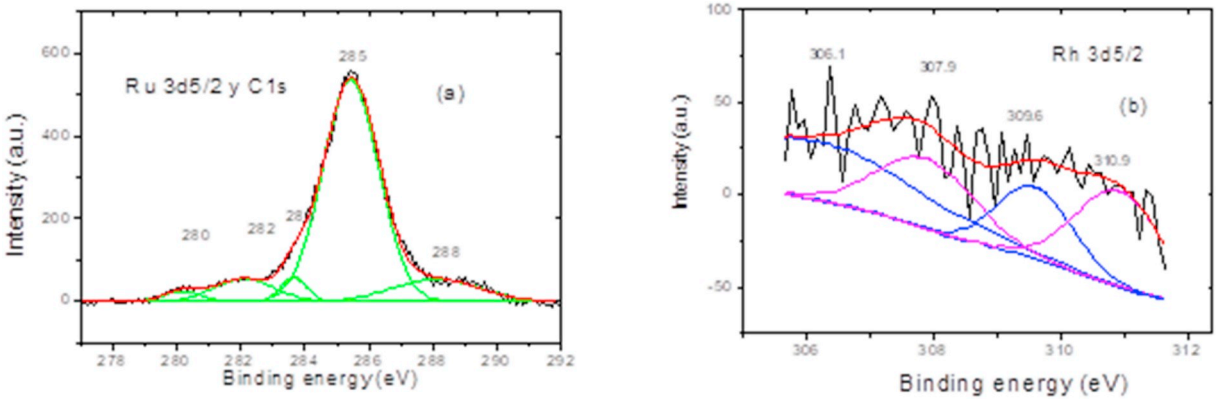

Fig. 8. XPS analysis of the 5%RuO_2–3Rh_2O_3/$AgNbO_3$ catalyst (a) Ru and (b) Rh.

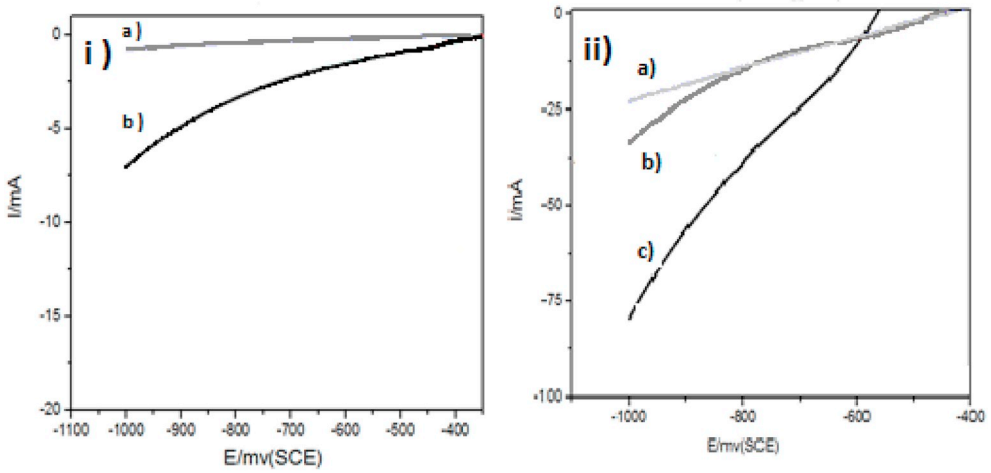

Fig. 9. The Linear Sweep Voltammetry (LSV) profile of the niobates synthesized in the present work. (i) Niobates: (a) $AgNbO_3$ and (b) $Ag_{0.5}NbO_3$. (ii) Catalysts of Ru–Rh supported on $Ag_{1-x}NbO_3$. (a)3%RuO_2–3%Rh_2O_3/$AgNbO_3$, (a) 5%RuO_2–3%Rh_2O_3/$AgNbO_3$, (c) 5%RuO_2–3%Rh_2O_3/$Ag_{0.5}NbO_3$.

2.4. Electrochemical evaluation of the materials

The electrochemical evaluation of the synthesized catalyst was carried out adding 3 mg of silver niobate catalyst to a solution composed of 6 μL of Nafion (Aldrich, 5 wt%), 60 μL of ethanol (Desarrollo de Especialidades Quìmicas (DEQ), 99.6%), and 30 μL of deionized water. Seeking to promote dispersion of the niobates, the solution was submitted to an ultrasound treatment during 60 min. Once the ultrasound treatment ended, 30 μL of the final solution was deposited onto an ITO plate (8–12 $\Omega \cdot sq^{-1}$ and A = 1.0 cm^2) and we waited until observing the complete evaporation of the liquid at room temperature. Later, this plate was utilized as a working electrode in a compound electrochemical cell with the carbon and Saturated Calomel Electrode (SCE) used as auxiliary and reference electrode, respectively. These electrodes were placed in contact with a solution of Na_2SO_4 (0.5 M) utilized as electrolyte. Prior to applying the current, the solution in contact with the electrodes was purged with argon during 3 min. The *i-E* profiles were performed in VersaStat version 3 equipment with an interval of 0.0–1.0 V, employing Linear Sweep Voltammetry (LSV) at a sweep velocity of 5 mV s^{-1}.

3. Results

3.1. Physicochemical characterization of the niobates

3.1.1. X-ray powder diffraction

The Fig. 1 depicts the X-Ray powder diffraction (XRD) of the silver niobates prepared by means of the solid-state route at 900 °C. In the x-ray diffraction spectra (Fig. 1a), it can be observed that in the 2θ = 20–80 interval, the main reflections are observed of the prepared materials (2θ = 31.894, 32.298, 39.5875, 39.8991, 46.007, 46.396, 46.644, 57,090, 57.563, 57.854, 67.598, 76.443, and 77.390), attributed to the JCPD 01–073–8073 card, which ensures the obtaining of a pure material, corresponding to the orthorhombic crystalline system. This arrangement is different from that reported by other authors [21, 22], The transformation is associated with the type of precursors employed, because the transition phases of the $AgNbO_3$ are already known and the atomic and physiochemical characteristics are in terms of the temperature [17–19]. In addition, at temperatures above 850 °C, the silver content of the structure increases, contributing to the symmetry of the crystalline arrangement-of-interest [23] (see Fig. 1).

Thermodynamic viability for obtaining $AgNbO_3$ at temperatures near 900 °C permitted the establishment of this temperature for studying the effect of the silver content on the $Ag_{1-x}NbO_3$, where X = 0.1 and 0.5. The results of the XRD are shown in Fig. 1b and c. For the first case, can be observed that the decrease of the silver content in the crystalline arrangement of the $AgNbO_3$ does not cause structural changes. This result is not in agreement with the one reported by A. Kania, who demonstrated the development of the reflections 2θ = 28, 54, and 67, as a result of a delay in the diffusion of the materials during the transition of the phases. If the reaction takes place at a higher temperature, there is the possibility of sublimation of the niobium, and of the increase in the concentration of silver [22]. With respect to the $Ag_{0.5}NbO_3$ material, it is evident that subtraction of silver leads to a re-ordering of the material, promoting the mixture of phases $AgNbO_3$ and $Ag_2Nb_2O_{11}$ (monoclinical,

01–078–5128).

3.1.2. Band gap energy

The results of the optical characterization of the synthesized niobates at 900 °C presented band gap values of 2.65 eV (Fig. 2). This value is slightly less than that reported in other works, that is, 2.8 ± 0.1 eV [24].

According to Hideki K. et al. $AgNbO_3$ possesses very similar optical and structural characteristics to those of $NaNbO_3$ and $NaTaO_3$, but its luminescent character makes it poorly competitive for optical applications, thus the need to impregnate it with metals [25]. The $Ag_{0.5}NbO_3$ system includes a shift toward the ultraviolet (UV) region, but the value is nearer that of the stoichiometric niobate. In contrast, in the $Ag_{0.5}NbO_3$ sample, the Eg is associated with the presence of vacancies in its structure due to silver deficit. It is possible that this action affects the energy of delocalization of the electrons and leads to a band gap energy shift up to 2.4 eV [25].

From the optical and structural characterization, significant differences were not observed amongst samples $AgNbO_3$ and $Ag_{0.9}NbO_3$. From the next section, the comparative study will only continue between the $AgNbO_3$ and $Ag_{0.5}NbO_3$ supports obtained by the solid-state route at 900 °C.

3.1.3. Transmission Electronic Microscopy (TEM)

In Fig. 3a–d, TEM images of both samples are presented. According to the images, we are able to observe that the support with perovskite structure is an agglomerate constituted of particles smaller than 10 nm. The elemental analysis indicates that for Ag, Nb, and O, the molar ratio is very near to 1:1:3, but the interplanar distances (0.278 nm) reveal that on the support segregated spherical particles of Ag_2O (0.243 nm) are found [4]. The morphology obtained in this work differs from that reported for ABO_3-type perovskites, which are principally constituted of agglomerated blocks and staircases are observed on their borders [17,20,26]; therefore, the use of silver obtained by electrolytic process is determinant in terms of the morphological characteristics of the catalyst. In the case of the $Ag_{0.5}NbO_3$ support, the morphology corresponds to a rectangular prism of several nanometers in length that is characteristic of double perovskites and is in agreement with the result of XRD (see Fig. 3c). The interplanar distance of this support was of 0.307 nm and is according with the elemental analysis for $Ag_2Nb_4O_{11}$ structure which the experimental Ag/Nb ratio is 6.45 as result of the evaporation of the niobate.

3.2. Characterization of the active phase (RuO_2–Rh_2O_3)

In this sections is shown the characterization of the decoration of $AgNbO_3$ and $Ag0.5NbO_3$ with metallic nanoparticles based on the reversible oxidation state (+3, +4) of the Rh ions in alloy with RuO_2, it could be an important factor to increase H_2 evolution for electrocatalysts [27].

3.2.1. TEM-EDS

In Fig. 4, the most representative images are shown for catalyst of constant metallic charge of 3%wt of Rh_2O_3 and varying the content of RuO_2 (1, 3, and 5%wt) calcined at 400 °C in an air atmosphere.

Fig. 4a corresponds to the nominal-charge of 1%RuO_2–3%Rh_2O_3/$AgNbO_3$ catalyst. According to the chemical analysis (Fig. 4b), the particle shown contains in average 8.60%wt RuO_2 and 4.20%wt of Rh_2O_3 corresponding to the $RuO_2/Rh_2O_3 = 2.0$ ratio. For the 1%RuO_2-3% Rh_2O_3/$Ag_{0.5}NbO_3$ catalyst, the chemical analysis revealed that the metallic charge was 1.55%wt RuO_2 and 0.72%wt Rh_2O_3 ($RuO_2/Rh_2O_3 = 2.15$). Image 4e corresponds to the 3%RuO_2-3% Rh_2O_3/$Ag_{0.5}NbO$ system; elemental analysis by EDS indicates that the surface demonstrated corresponds to the agglomerated nanoparticles of RuO_2, because the interplanar distance corresponds to 0.17 nm corresponding to the face (2,1,1), which is characteristic of these crystalline nanoparticles [28].

3.2.2. X-ray photoelectron spectroscopy (XPS)

In Fig. 5(a–d) are depicted the characteristic high resolution narrow spectra for Ag 3d5/2, Nb 3d5/2, O 1s and C 1s region for AgNbO3 compared to the $Ag_{0.5}NbO_3$ support, from spectra were determined the elemental chemical composition in the materials surface. It is clear that both samples present slight differences in chemical shifts mainly in Nb, Ag and O reflecting changes in chemical environment due to changes in chemical states. It is important to note that the proportion incorporated of Ag in the support is promotes the structural changes. The narrow spectra for O 1s is very clear, in Fig. 5c can be seen the main peak, located at 531.7 and 532 eV for $Ag0.5NbO_3$ and $AgNbO_3$ respectively.

Analyzing spectra in detail, changes in spectra of the $AgNbO_3$ and $Ag_{0.5}NbO_3$ supports were observed, from Fig. 6(a–d) is observed that Nb spectra is more intense when Ag content is low, this could be attributed to a structure distortion with Ag increases. The spectrum of Nb 3d5/2 region shows two main doublets, one doublet with peaks located at 205.6 and 208.4 eV and the other doublet with peaks located in 206.7 and 209.7 eV, attributed to Nb in Nb_2O_3 and the Nb in the $Ag_{0.5}NbO_3$ structure respectively, as can be seen in Fig. 6 (a). The spectrum of Nb 3d5/2 region in Fig. 6 (b) shows two doublets which have a slight shift, one doublet located in 205.2 and 209.6 eV attributed to the Nb in Nb_2O_3 and the other doublet located in 207.3 and 211.5 eV due to the Nb in $AgNbO_3$. Spectra of Ag 3d5/2 region reveal three main doublets, the first doublet located in 366 and 372.8 eV, the second doublet in 367.3 and 373.8 eV and the third doublet in 370 and 375.2 eV as is observed in Fig. 6 (c) and (d), this doublets were attributed most probably to the Ag as Ag_2O, Ag in the niobate (Ag_xNbO_3) and some Ag + that is outside to the niobate structure.

As part of the characterization of the chemical state and of the electronic structure of the Ru–Rh catalysts, the elemental chemical composition of the electrocatalysts was determined (see Table 1). The results indicate that the amount of RuO_2 dispersed was greater than the nominal charge ($1.40 > RuO_2/Rh_2O_3 < 2.83$) for the $AgNbO_3$ support, while in the other supports, a lesser nominal amount of RuO_2 ($RuO_2/Rh_2O_3 = 0.95$) was observed. This is supported by the TEM image 4a, in which RuO_2 nanoparticles are presented.

In Fig. 7, the characteristic spectrum of catalyst 1%RuO_2–3Rh_2O_3/$AgNbO_3$ is shown. By means of this technique, the presence of Ru is confirmed in the 278–282 eV interval, highlighting the characteristic signal of 279.7 eV and that is associated with the presence of RuO_2 [18,29] and the 281.4 eV related to the RuO_3, while the most outstanding signal of rhodium is found slight shift at 307.2 eV and is associated with Ru_2O_3, a signal in 308.4 eV attributed to the $RuRh_2O_4$ and the 309.2 eV attributed to $RhNbO_4$ [30]. Fig. 8 shows the spectrum for the catalyst 5% RuO_2–3Rh_2O_3/$AgNbO_3$, similar peaks were found, it seems that the peak located at 309.8 eV, which was attributed to the Rh in the $RuRh_2O_4$ is slightly lower in this catalyst than the observed in the catalyst with 1% of Ru.

3.3. Electrochemical tests

Fig. 9 depicts the results of the linear sweep voltammetry, in which the profiles of current vs. potential can describe a Hydrogen Evolution Reaction (HER). In Fig. 9, it can be appreciated that the supports ($AgNbO_3$ and $Ag_{0.5}NbO_3$) present a response in the faradaic current; however, one may clearly observe an increase in such a response when the Ag content in the support diminished. This behavior can be attributed to the absence of Ag_2O nanoparticles dispersed in the support, in addition to the structural disorder due to the presence of the phases of $AgNbO_3$ (orthorhombic) and $Ag_2Nb_4O_{11}$ (monoclinical) in the non-stoichiometric sample. According to D. Woodward et al., $Ag_2Nb_4O_{11}$ is not constituted solely of octahedrons that share corners, but it is also composed of NbO_7 polyhedrons with shared and distorted borders at the corners containing regular octahedrons of NbO_6 and probably it improves the electrical response [31].

Fig. 9b reveals that the presence of the co-catalyzers of Rh–Ru in

different atomic ratios increases, at around five times the order-of-magnitude, the response of the current supported in $AgNbO_3$, remarking that the response of the faradaic current is observed as increased in terms of the content of RuO_2.

For the case of the sample in which the active phase is supported in a mixture of phases ($5\%RuO_2$–$3\%Rh_2O_3/Ag_{0.5}NbO_3$), a notable increase in the response of the faradaic current was observed (10 times) respect to the non-impregnated sample ($Ag_{0.5}NbO_3$). This current was more than double compared with the best bimetallic electrocatalyst supported on stoichiometric silver niobate ($5\%RuO_2$–$3\%Rh_2O_3/AgNbO_3$). This result could probably be associated with a homogeneous dispersion of the metallic phases as RuO_2 and $RuRh_2O_4$ recognized with XPS analysis. This hypothesis is supported by the elemental atomic composition shown in Table 1, where the RuO_2/Rh_2O_3 ratios around 1.32 played a positive role in improving the performance of HER, especially for the $5.0\%RuO_2$–$3Rh_2O_3/Ag_{0.5}NbO_3$. J. M. Sieven has claimed reduction potential shifts towards a more negative potential due to the formation of more stable complexes of Ru (II) and Rh (III) to promote a better interaction support-metals and empowering the electronic properties of the system in the HER [32]. Finally, it is noted that the good HER activity of $5.0\%RuO_2$–$3Rh_2O_3/Ag_{0.5}NbO_3$, depicts an important improvement in HER activities for niobates systems, but their performances were less attractive in comparison with commercial Pt–C electrode previously reported (current density $\leq 100\,mA\,cm^{-2}$, over potential ≤ 120 mV and total slope $< 50\,mV.dec^{-1}$) [33–35].

4. Conclusions

In this work, it was evidenced that the modification of the Ag/Nb ratio in the $AgNbO_3$ system synthesized by solid state at 900 °C gave rise to optical and structural changes in the X = 0–0.5 interval. It is noteworthy that the absence of silver caused a structural evolution toward a double perovskite structure and a shift of 0.2 eV toward the visible region (2.4 eV). Both systems ($AgNbO_3$ and $Ag_{0.5}NbO_3$) were impregnated with different RuO_2/Rh_2O_3 ratios and were evaluated electrochemically. The results revealed increases of around 2.5-times the orders-of-magnitude of the bimetallic system supported on $Ag_{0.5}NbO_3$ with respect to the current supported on $AgNbO_3$, remarking that the response of the faradaic current increased in terms of the content of RuO_2, as indicated by the $5\%RuO_2$–$3\%Rh_2O_3/Ag_{0.5}NbO_3$ system as the result of better interaction between the support and the active phase.

Declaration of competing interest

None.

Acknowledgements

The authors are grateful to the Materials Construction Laboratory of FIC-UANL for the facilities lent in the development of these materials and M.C. Viridiana Maturano Rojas from ICAT-UNAM for TEM analysis. CARR thanks CONACYT for the support granted through Masters-degree scholarship, a mixed scholarship, and the Nanoscience and Nanotechnology Network from CONACYT.

References

[1] M.L. Ávalos Rodríguez, J.J. Alvarado Flores, J.V. Alcaraz Vera, J.G. Rutiaga Quiñones, J. Espino Valencia, The legal regulation of the H2 as a strategy for public policy in n Mexico from the consolidation of the National Council of the hydrogen, Int. J. Hydrogen Energy 44 (24) (2019) 12303–12308, https://doi.org/10.1016/j.ijhydene.2018.09.214.

[2] L. Rengui, Latest progress in hydrogen production from solar water splitting via photocatalysis, photoelectrochemical, and photovoltaic-photoelectrochemical solutions, Chin. J. Catal. 38 (1) (2017) 5–12, https://doi.org/10.1016/S1872-2067(16)62552-4.

[3] H. Pan, Principles on design and fabrication of nanomaterials as photocatalysts for water-splitting, Renew. Sustain. Energy Rev. 57 (2016) 584–601, https://doi.org/10.1016/j.rser.2015.12.117.

[4] T. Ahmad, U. Forooq, R. Phul, Fabrication and photocatalytic applications of perovskite materials with special emphasis on alkali-metal-based niobates and tantalates, Ind. Eng. Chem. Res. 58 (2018) 18–41, https://doi.org/10.1021/acs.iecr.7b04641.

[5] N.M. Gupta, Factors affecting the efficiency of a water splitting photocatalyst: a perspective, Renew. Sustain. Energy Rev. 71 (2017) 585–601, https://doi.org/10.1016/j.rser.2016.12.086.

[6] F.E. Osterloh, Inorganic material as catalysts for photochemical splitting of water, Chem. Mater. 20 (1) (2008) 35–54, https://doi.org/10.1016/j.jphotochemrev.2011.07.001.

[7] D.L. Serna, S.I. Suarez-Vazquez, J.C. Duran-Alvarez, R. Zanella, V.H. Guerra, A. Cruz-Lopez, Kinetic syudy of photocatalytic degradation of the emerging contaminant bisphenol A using N-TiO_2 in visible light: a study of the significance of dissolved oxygen, Reac. Kinet. Mech. Cat. 122 (2017) 1655–1670, https://doi.org/10.1007/s11144-017-1200-4.

[8] Y. Moriya, T. Takata y, K. Domen, Recent progress in the development of (oxy) nitride photocatalysts for water splitting under visible-light irradiation, Coord. Chem. Rev. 257 (2013) 1957–1969, https://doi.org/10.1016/j.ccr.2013.01.021.

[9] L. Yang, J. Liu, H. Chang, Sh Tang, Enhancing the visible-light-induced photocatalytic activity of $AgNbO_3$ by loading Ag@AgCl nanoparticles, R. Soc. Chem. 5 (2015) 59970, https://doi.org/10.1039/C5RA06803G.

[10] K. Maeda, Photocatalytic water splitting using semiconductor particles: history and recent developments, J. Photochem. Photobiol. C Photochem. Rev. 12 (4) (2011) 237–268, https://doi.org/10.1016/j.jphotochemrev.2011.07.001.

[11] C. Prasad, H. Tang, Q. Qin Liu, S. Zulfiqar, S. Shah, I. Bahadur, An overview of semiconductors/layered double hydroxides composites: properties, synthesis, photocatalytic and photoelectrochemical applications, J. Mol. Liq. 289 (2019) 111114, https://doi.org/10.1016/j.molliq.2019.111114.

[12] J.-P. Boilot, T. Gacoin, S. Perruchas, Synthesis and sol-gel assembly of nanophosphors, Compt. Rendus Chem. 13 (1–2) (2010) 186–198, https://doi.org/10.1016/j.crci.2009.03.008.

[13] G. Ya Grodziuk, N.D. Shcherban, V.V. Shvalagin, A.V. Korzhak, N.S. Andryushina, M.A. Skoryk, S. Ya Kuchmiy, Int. J. Hydrogen Energy 42 (38) (2017) 24108–24116, https://doi.org/10.1016/j.ijhydene.2017.07.238.

[14] Yuchao Hu, Gaosheng Li, Shichao Zong, Jinwen Shi, liejin Guo, Self-assemble nanohybrid of cadmium sulfide and calcium niobate: photocatalyst with enhanced charge separation for efficient visible light induced hydrogen generation, Catal. Today 315 (2018) 117–125, https://doi.org/10.1016/j.cattod.2018.03.037.

[15] A. Kudo, Y. Miseki, Heterogeneous photocatalyst materials for water splitting, Chem. Soc. Rev. 38 (2009) 253–278, https://doi.org/10.1039/b800489g.

[16] Yen Fan, Fang Wang, Chenchen Meng, Lijie Bai, Junying Li, Pingxing, batao teng, Leihong Zhao, Bai Song, Crystalline phase engineering on cocatalysts: a promising approach to enhancement on photocatalytic conversion of carbon dioxide to fuels, Appl. Catal. B Environ. 230 (2018) 145–153, https://doi.org/10.1016/j.apcatb.2018.02.046.

[17] Y. Lu, Q. Shen, Q. Yu, F. Zhang, G. Li, W. Zhang, Photoinduced in situ growth of Ag nanoparticles on AgNbO3, J. Phys. Chem. C (2016) 28712–28716, https://doi.org/10.1021/acs.jpcc.6b10961.

[18] A. Cruz-López, A. C, Limón Pozos, S. Iván Suárez Vázquez, R. Zanella, R. Gómez, Zn-Ge oxynitride based nano.photocatalyst for hydrogen production under visible light, Mater. Res. Bull. 83 (2016) 603–608, https://doi.org/10.1016/j.materresbull.2016.07.013.

[19] M. Antuch, P. Millet, A. Iwase, A. Kudo, S.A. Grigoriev, Y.Z. Voloshin, Characterization of Rh:SrTiO3 photoelectrodes surface-modified with a cobalt clathrochelate and their application to the hydrogen evolution reaction, Electrochim. Acta 258 (2017) 255–265, https://doi.org/10.1016/j.electacta.2017.10.018.

[20] U.A. Joshi, A. Palasyuk, D. Arney, P.A. Maggard, Semiconducting oxide to facilitate the conversion of solar energy to chemical fuels, J. Phys. Chem. Lett. 1 (2010) 2719–2726, https://doi.org/10.1021/jz100961d.

[21] Huoming Shu, Jimin Xie, Hui Xu, Huaming Li, Zheng Gu, Guangsons Sun, yuanguo Xu, Hydrogen dynamics in HiPco carbon nanotubes, J. Alloy. Comp. 406 (2010) 633–637, https://doi.org/10.1016/j.jallcom.2004.11.102.

[22] A. Kania, A. Niewiadomski, S. Miga, I. Jankowska-Sumara, M. Pawlik, Z. Ujma, J. Koperski, J. Sushanicz, Silver deficiency and excess effect on quality, dielectric properties and phase transitions of $AgNbO_3$ ceramics, J. Eur. Ceram. Soc. 34 (2014) 1761–1770, https://doi.org/10.1016/j.jeurceramsoc.2014.01.016.

[23] Tingsong Zhang, Chenyang Zhang, Ling Wang, Yisheng Chai, Shipeng Shen, Young Sun, HongmingYuan, Shouhua Feng, Low-temperature phase transition in $AgNbO_3$, J. Am. Ceram. Soc. 97 (2014) 1895–1898, https://doi.org/10.1111/jace.12857.

[24] Ch Wang, J. Yang, X. Wu, Y. Song, G. Cai, H. Xu, J. Zhu, H. Li, Synthesis and characterization of $AgBr/AgNbO_3$ composite with enhanced visible-light photocatalytic activity, Appl. Surf. Sci. 273 (2013) 159–166, https://doi.org/10.1016/j.apsusc.2013.02.004.

[25] H. Kato, H. Kobayashi, A. Kudo, Role of Ag+ in the band structures and photocatalytic properties of AgMO3 (M: Ta and Nb) with the perovskite structure, J. Phys. Chem. B 106 (48) (2002) 12441–12447, https://doi.org/10.1021/jp025974n.

[26] D. Arney, Ch Hardy, B. Greve, P.A. Maggard, Flux synthesis of $AgNbO_3$: effect of particle surfaces and sizes on photocatalytic activity, J. Photochem. Photobiol. A Chem. 214 (2010) 54–60, https://doi.org/10.1016/j.jphotochem.2010.06.006.

[27] Y. Sasaki, H. Nemoto, K. Saito, A. Kudo, Solar water splitting using powdered photocatalyst driven by Z-schematic interparticle electron transfer without an electron mediator, J. Phys. Chem. C 113 (40) (2009) 17536–17542, https://doi.org/10.1021/jp907128k.

[28] R. Thangappan, M. Arivanandhan, R. Dhinesh Kumer, R. Jayavel, Facile synthesis of RuO2nanoparticles anchored on graphene nanosheets for high performance composite electrode for supercapacitor applications, J. Phys. Chem. Solids 121 (2018) 339–349, https://doi.org/10.1016/j.jpcs.2018.05.049.

[29] F.A. Rodríguez, E.P. Rivero, L. Lartundo-Rojas, I. González, Preparation and characterization of Sb_2O_5-doped Ti/RuO_2-ZrO_2 for dye decolorization by means of active chlorine, J. Solid State Electrochem. 18 (2014) 3153–3162, https://doi.org/10.1007/s10008-014-2554-4.

[30] L.S. Kibis, A.I. Stadnichnko, S.V. Koscheev, V.I. Zaikovskii, A.I. Boronin, XPS study of nanostructured rhodium oxide film comprising Rh^{4+} species, J. Phys. Chem. C 120 (2016) 19142–19150, https://doi.org/10.1021/acs.jpcc.6b05219.

[31] D. Woodward, M.R. Lees, P.A. Thomas, Structural phase transition in the $Ag_2Nb_4O_{11}$-$Na_2Nb_4O_{11}$ solid solution, J. Solid State Chem. 192 (2012) 385–389, https://doi.org/10.1016/j.jssc.2012.04.014.

[32] J.M. Sieben, M.M.E. Duarte, C.E. Mayer, Efecto de aditivos orgánicos en la depositación de catalizadores Pt/Ru, Rev. Mater. 15 (1) (2010) 76–87.

[33] Zhuo Zhuojun Duan, Mingyu Pi, Dingke Zhang, Peng Zhang, Junkai Deng, Shijian Chen, High Hydrogen evolution performance of Al doped CoP_3 nanowires arrays with high stability in acid solution superior to Pt/C, Int. J. Hydrogen Energy 4 (2019) 8062–8069, https://doi.org/10.1016/j.ijhydene.2019.02.095.

[34] J. Ma, A. Hibrioux, N. Alonso-Vante, Enhanced HER and ORR behavior on photodeposited Pt nanoparticles onto oxide.carbon composite, J. Solid State Electrochim. 17 (1) (2013) 1913–1921, https://doi.org/10.1007/s10008-013-2046-y.

[35] Reza Kivian, Sang-il Choi, Jinho Park, Tianyuan Liu, Hsin-Chen Peng, Ning Lu, Jinguo Wang, Moon J. Kim, Younan Xia, Seung Woo Lee, Pt-Ni octahedral nanocrystals as a class of highly active electrocatalyst toward the hydrogen evolution reaction in alkaline electrolyte, J. Mater. Chem. A 4 (2016) 12396–12397, https://doi.org/10.1039/c6ta05411k.